Chiral Borospherenes

Deutsche Ausgabe: DOI: 10.1002/ange.201501588
Internationale Ausgabe: DOI: 10.1002/anie.201501588

Cage-Like B_{41}^+ and B_{42}^{2+}: New Chiral Members of the Borospherene Family**

Qiang Chen, Su-Yan Zhang, Hui Bai, Wen-Juan Tian, Ting Gao, Hai-Ru Li, Chang-Qing Miao, Yue-Wen Mu, Hai-Gang Lu, Hua-Jin Zhai,* and Si-Dian Li**

Abstract: *The newly discovered borospherenes $B_{40}^{-/0}$ and B_{39}^- mark the onset of a new class of boron nanostructures. Based on extensive first-principles calculations, we introduce herein two new chiral members to the borospherene family: the cage-like C_1 B_{41}^+ (**1**) and C_2 B_{42}^{2+} (**2**), both of which are the global minima of the systems with degenerate enantiomers. These chiral borospherene cations are composed of twelve interwoven boron double chains with six hexagonal and heptagonal faces and may be viewed as the cuborenes analogous to cubane (C_8H_8). Chemical bonding analyses show that there exists a three-center two-electron σ bond on each B_3 triangle and twelve multicenter two-electron π bonds over the σ skeleton. Molecular dynamics simulations indicate that C_1 B_{41}^+ (**1**) fluctuates above 300 K, whereas C_2 B_{42}^{2+} (**2**) remains dynamically stable. The infrared and Raman spectra of these borospherene cations are predicted to facilitate their experimental characterizations.*

Buckminsterfullerene C_{60} has been a superstar in chemistry and materials science ever since its discovery in 1985.[1] It pioneers the route to the nowadays popular carbon nanotubes and graphenes.[2,3] Synthesis of the first axially chiral D_2 C_{76} in 1991 highlights the importance of chirality in elemental nanoclusters and nanostructures. However, only a handful of free-standing cage-like clusters have been characterized experimentally before 2014, including Au_{16}^-,[4] stannaspherene Sn_{12}^{2-},[5] and plumbaspherene Pb_{12}^{2-}.[6] As the lighter neighbor of carbon in the periodic table, boron is a typical electron-deficient element. Its chemistry is dominated by multicenter two-electron bonds (*m*c-2e) in both boron solids and polyhedral molecules. The possibility of all-boron fullerenes was not considered for over two decades before the celebrated I_h B_{80} buckyball was proposed in 2007,[7] which was built upon the C_{60} motif by capping the 20 surface hexagons. However, B_{80} was later found to favor core–shell structures at various theoretical levels.[8,9] In contrast to bulk boron, small boron clusters $B_n^{-/0}$ have been experimentally confirmed to be planar or quasi-planar in an unprecedented wide range of sizes (n = 3–25, 30, 35, 36),[10–21] including the chiral quasi-planar C_1 B_{30}^-,[17] unveiling a flat world of boron. Small boron dihydride clusters $B_nH_2^{-/0}$ (n = 4–12) have proven to be planar boron double-chains (BDCs) with two hydrogen terminals in both theory and experiment,[22,23] demonstrating the importance of BDCs as building units in the low-dimensional boron nanostructures. Various two-dimensional boron nanostructures composed of interwoven BDCs have also been investigated theoretically,[24–26] but none has been experimentally confirmed. The first all-boron fullerenes D_{2d} $B_{40}^{-/0}$, referred to as borospherenes in literature, were discovered in 2014 in a combined experimental and computational study,[27] marking the onset of the borospherene chemistry. The D_{2d} $B_{40}^{-/0}$ borospherenes are composed of twelve interwoven BDCs with two hexagon holes on the top and at the bottom and four heptagon holes on the waist, slightly elongated along the C_2 main axis. Although D_{2d} B_{40}^- is slightly less stable than the quasi-planar global minimum (GM) C_s B_{40}^- of the mono-anion, the neutral D_{2d} B_{40} proves to be the well-defined GM with a huge energy gap of 3.13 eV between its highest occupied molecular orbital (HOMO) and lowest unoccupied molecular orbital (LUMO).[27] D_{2d} B_{40} possesses a unique bonding pattern of σ plus π double delocalization: 96 of its 120 valence electrons are delocalized in 48 three-center two-electron (3c–2e) σ bonds and 24 are delocalized in 12 *m*c-2e π bonds (four 5c–2e π, four 6c–2e π, and four 7c–2e π), rendering three-dimensional aromaticity for this cage-like molecule. Closely following D_{2d} $B_{40}^{-/0}$, the first axially chiral borospherenes C_3/C_2 B_{39}^- were observed.[28] Endohedral and exohedral metalloborospherenes M@B_{40} (M = Ca, Sr) and M&B_{40} (M = Be, Mg) were also predicted to be viable species, further supporting the robustness of the B_{40} borospherene.[29] Very recently, a theoretical study of the electronic structure and electronic spectra of D_{2d} B_{40} and a computational study of the endohedral metalloborospherenes M@B_{40} (M = Sc, Y, and La) were reported.[30,31]

Based on extensive GM searches and first principles calculations, we introduce herein two new cationic chiral members to the borospherene family, the C_1 B_{41}^+ (**1**) monocation and C_2 B_{42}^{2+} (**2**) dication, both of which are the

[*] Q. Chen, S.-Y. Zhang, H. Bai, W.-J. Tian, T. Gao, H.-R. Li, Dr. Y.-W. Mu, H.-G. Lu, Prof. Dr. H.-J. Zhai, Prof. Dr. S.-D. Li
Nanocluster Laboratory, Institute of Molecular Science
Shanxi University
Taiyuan 030006 (China)
E-mail: luhg@sxu.edu.cn
hj.zhai@sxu.edu.cn
lisidian@sxu.edu.cn
Q. Chen, C.-Q. Miao
Institute of Materials Science and Department of Chemistry,
Xinzhou Teachers' University
Xinzhou 034000 (China)

[**] This work was supported by the National Natural Science Foundation of China (21243004, 21373130), the Shanxi International Cooperation project (2013081018), and the State Key Laboratory of Quantum Optics and Quantum Optics Devices (KF201402). H.J.Z. gratefully acknowledges the start-up fund from Shanxi University for support.

Supporting information for this article is available on the WWW under http://dx.doi.org/10.1002/anie.201501588.

 © 2015 Wiley-VCH Verlag GmbH & Co. KGaA, Weinheim

global minima of the systems with degenerate enantiomers. Characterized with the bonding pattern of σ plus π double delocalization, these cage-like boron clusters are also composed of twelve interwoven BDCs with six hexagonal and heptagonal faces and may be viewed as cuborenes analogous to cubane (C_8H_8). C_1 B_{41}^+ (**1**) exhibits obvious structural fluctuations during the molecular dynamics simulations above 300 K, similar to C_3/C_2 B_{39}^-, whereas C_2 B_{42}^{2+} (**2**) remains dynamically stable above room temperatures, analogous to D_{2d} B_{40}. The infrared (IR) and Raman spectra of the two chiral borospherene cations are predicted to facilitate their future experimental characterizations.

Extensive GM structural searches were performed for B_{41}^+ and B_{42}^{2+} employing the minima hopping (MH) algorithm[9,32] at the density functional theory (DFT) level, combined with manual structural constructions based on the known planar, cage-like, and tubular boron clusters. Low-lying structures were then fully optimized and their relative energies evaluated at both the hybrid PBE0[33] and CAM-B3LYP[34] levels with the 6-311 + G* basis set[35] implemented in Gaussian 09 suite.[36] CAM-B3LYP includes long-range corrections using the Coulomb attenuating method. The relative stabilities of the three lowest-lying isomers were further refined using the more accurate coupled cluster method with triple excitations (CCSD(T))[37–39] implemented in MOLPRO[40] using the 6-31G(d) basis set at the PBE0 geometries. The optimized structures of the chiral borospherene cations C_1 B_{41}^+ (**1**) and C_2 B_{42}^{2+} (**2**) and their degenerate enantiomers C_1 B_{41}^+ (**1′**) and C_2 B_{42}^{2+} (**2′**) are depicted in Figure 1. The configurational energy spectra of the two cations within 1.5 eV at PBE0 are shown in Figure 2. More alternative isomers are summarized in the Supporting Information in Figure S1 for B_{41}^+ and Figure S2 for B_{42}^{2+}.

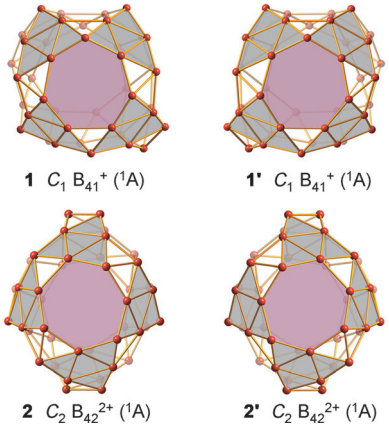

Figure 1. Optimized structures of the chiral borospherene cations C_1 B_{41}^+ (**1**) and C_2 B_{42}^{2+} (**2**) and their degenerate enantiomers C_1 B_{41}^+ (**1′**) and C_2 B_{42}^{2+} (**2′**). The frontal B_7 heptagons are highlighted in purple and the close-packed B_6 triangles in gray.

We started our structural searches from a cage-like B_{41}^+ manually constructed by replacing one B_6 hexagon on D_{2d} B_{40} with a B_7 heptagon, followed by a full structural optimization. The optimized low-symmetry C_1 B_{41}^+ (**1**) turns out to be a true minimum of the monocation with the lowest vibrational

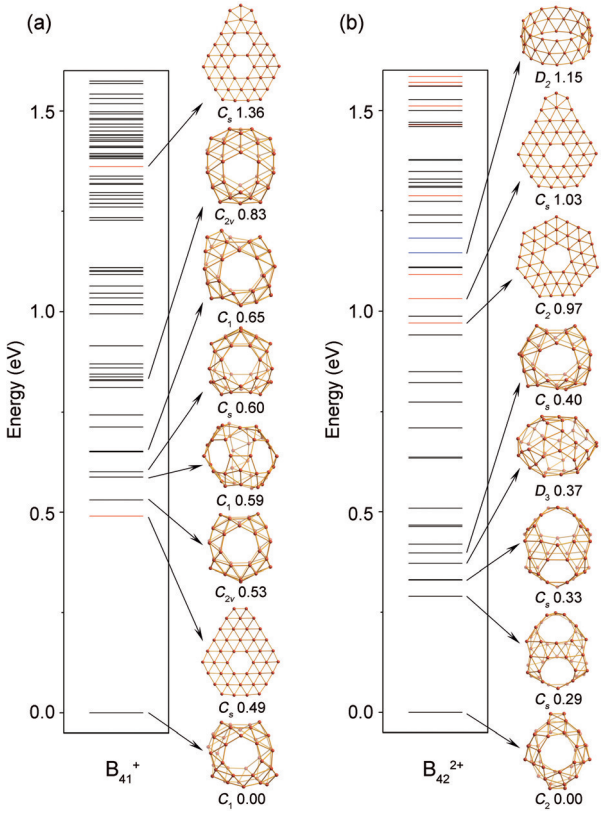

Figure 2. Configurational energy spectra of a) B_{41}^+ and b) B_{42}^{2+} at PBE0/6-311 + G* level. The energy of the global minimum is taken to be zero and the relative energies are in eV. The black, red, and blue bars denote fullerene-like cages, quasi-planar, and triple-ring tubular structures, respectively.

frequency of 158 cm^{-1} (a mode). Furthermore, this slightly distorted borospherene proves to be the GM on the basis of the MH searches: it lies 0.49 eV lower than the second lowest-lying quasi-planar C_s B_{41}^+ that can be derived from the experimentally observed B_{36} cluster[18,21] and 0.53 eV lower than the third lowest-lying cage-like C_{2v} B_{41}^+ that is a hexagon-face-capped D_{2d} B_{40} at the PBE0 level (Figures 2a and S1). At the CAM-B3LYP and CCSD(T) levels, C_1 B_{41}^+ (**1**) lies 0.82 and 0.78 eV lower than the second lowest-lying planar C_s isomer, respectively, further indicating that C_1 B_{41}^+ (**1**) is the well-defined GM of the system. It is known that PBE0 biases toward the quasi-planar or tubular structures, whereas CAM-B3LYP and the more reliable CCSD(T) favor cages.[28] However, all three levels of theory conclude that C_1 B_{41}^+ (**1**) is the first chiral borospherene monocation, along with its enantiomer. In fact, most of the low-lying B_{41}^+ isomers are cage-like, except the first quasi-planar C_s B_{41}^+ derived from the ground-state C_{6v} B_{36}[18,21] and the second quasi-planar C_s B_{41}^+ derived from the ground-state C_s B_{40}^- (Figure 2a).[27] Similar to D_{2d} B_{40}, C_1 B_{41}^+ (**1**) is composed of twelve interwoven BDCs, with one hexagon on the top, one heptagon at the bottom, and four heptagons on the waist. Alternatively, it can be viewed as a cubic box made of eight close-packed B_6 triangles propped by twelve interwoven BDCs. With 49 triangles, one hexagon, and five heptagons on the surface, C_1 B_{41}^+ (**1**) follows Euler's rule, which in this case reads: E(94

© 2015 Wiley-VCH Verlag GmbH & Co. KGaA, Weinheim

edges) = F(49 triangular + 1 hexagonal + 5 heptagonal faces) + V(41 vertices) − 2.

With both the two B_6 hexagons on the top and at the bottom of D_{2d} B_{40} replaced by B_7 heptagons, three cage-like isomers with six heptagons in different orientations are obtained at PBE0: the lowest-lying borospherene C_2 B_{42}^{2+} (**2**), the second lowest-lying C_s B_{42}^{2+} being 0.29 eV higher than C_2 (**2**), and the fourth lowest-lying D_3 B_{42}^{2+} being 0.37 eV above C_2 (**2**) (Figures 2b and S2). They are all true minima for the dication without imaginary vibrational frequencies. At CAM-B3LYP and CCSD(T), C_2 B_{42}^{2+} (**2**) turns out to be 0.30 and 0.28 eV lower than the second lowest-lying cage-like C_s B_{42}^{2+}, respectively, well supporting the PBE0 results. As the GM of the dication slightly elongated along its C_2 axis, C_2 B_{42}^{2+} (**2**) is an axially chiral borospherene degenerate with its enantiomer. It contains two heptagons on the top, two heptagons in the middle, and two heptagons at the bottom around the C_2 molecular axis. It can also be viewed as a cubic box made of eight close-packed B_6 triangles, supported by twelve interwoven BDCs. With 50 triangles and six heptagons, it conforms to Euler's rule: E(96 edges) = F(50 triangular + 6 heptagonal faces) + V(42 vertices) − 2. We also notice that all the low-lying isomers of B_{42}^{2+} within 0.9 eV possess cage-like structures, whereas the triplet planar C_s B_{42}^{2+} with a heptagon at the center, the singlet planar C_s B_{42}^{2+} with a hexagon at the center, and the triplet triple-ring tubular D_2 B_{42}^{2+} lie much higher (> 0.97 eV; Figure 2b).

The high stabilities of these borospherene cations originate from their unique electronic structure and bonding patterns. C_1 B_{41}^{+} (**1**) and C_2 B_{42}^{2+} (**2**) possess HOMO–LUMO energy gaps of 3.16 eV and 3.24 eV at PBE0, respectively, which are well comparable with the corresponding values of 2.89 eV for C_3 B_{39}^{-}, 3.13 eV for D_{2d} B_{40}, and 3.02 eV for I_h C_{60} obtained at the same theoretical level.[27,28] The large HOMO–LUMO gaps indicate the high stability of these cationic borospherenes in thermodynamics, whereas their neutrals C_1 B_{41} and C_2 B_{42}, with the LUMOs of the corresponding cations being singly or doubly occupied, are expected to be unstable in thermodynamics. This turns out to be true.

The bonding patterns of these closed-shell borospherene cations are analyzed using the AdNDP approach[41] which is an extension of the natural bond orbital (NBO) analyses to include the multicenter bonding elements. As shown in Figure 3a, C_1 B_{41}^{+} (**1**) possesses 41 3c–2e σ bonds on the 41 B_3 triangles along the interwoven BDCs, and eight 6c–2e σ bonds on the eight close-packed B_6 triangles at the eight corners. As the central B_3 triangles make the major contribution to the 6c–2e σ bonds, all the 49 σ bonds can be practically treated as 3c–2e bonds distributed on the twelve interwoven BDCs, with one 3c–2e σ bond on each B_3 triangle. The remaining 24 valence electrons can be classified into three 5c–2e π bonds and one 6c–2e π bond on the top and at the bottom, four 6c–2e π bonds on the waist, and four 7c–2e bonds on the top and at the bottom, in an overall symmetry of C_1. The twelve delocalized π bonds cover the cage surface almost evenly along the twelve interwoven BDCs. C_1 B_{41}^{+} (**1**) is thus characterized with a σ plus π double delocalization bonding pattern, similar to D_{2d} B_{40}.[27] Overall, although C_1 B_{41}^{+} (**1**) has one more 3c–2e σ bond than D_{2d} B_{40}, both of them have twelve delocalized π bonds over the cage surface.

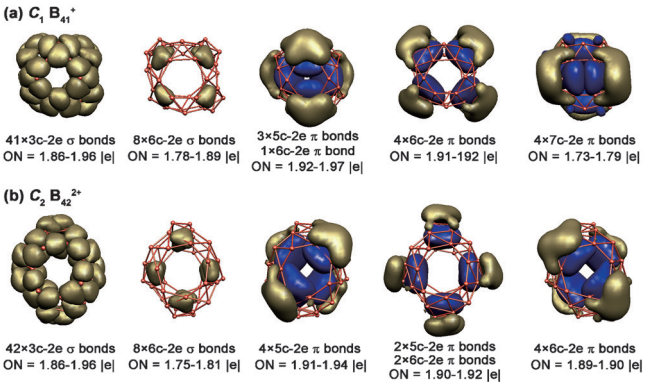

Figure 3. AdNDP bonding patterns of a) C_1 B_{41}^{+} (**1**/**1′**) and b) C_2 B_{42}^{2+} (**2**/**2′**), with the occupation numbers (ONs) indicated.

The bonding pattern of C_2 B_{42}^{2+} (**2**) is similar. As shown in Figure 3b, it has practically 50 delocalized 3c–2e σ bonds on 50 B_3 triangles and twelve delocalized π bonds distributed almost evenly over the twelve interwoven BDCs. The π bonds can be classified into three sets: four 5c–2e π bonds on the top and at the bottom, two 5c–2e π bonds and two 6c–2e π bonds on the waist, and four 6c–2e π bonds on the top and at the bottom. C_2 B_{42}^{2+} (**2**) is thus again characterized with a σ plus π double delocalization bonding pattern. Although it has two more 3c–2e σ bonds than D_{2d} B_{40} and one more 3c–2e σ bond than C_1 B_{41}^{+} (**1**), these borospherenes all have twelve delocalized π bonds over the cage surface. The chiral C_3/C_2 B_{39}^{-},[28] achiral D_{2d} B_{40},[27] chiral C_1 B_{41}^{+} (**1**), and chiral C_2 B_{42}^{2+} (**2**) thus form a π-isovalent B_n^q series in different charge states ($q = n - 40$), which all have twelve delocalized multicenter π bonds (twelve mc-2e π bonds, $m = 5, 6, 7$) over a σ skeleton made of $n + 8$ delocalized three-center σ bonds ($n + 8$ 3c–2e σ bonds, 8 represents the eight central B_3 triangles at the corners of a cubic box; see Figure S3). These perfect or slightly distorted cubic-box borospherenes with six hexagon or heptagon faces surrounded by twelve interwoven BDCs are the boron analogues of the cubane (C_8H_8) and may be viewed as cuborenes with eight B_6 triangles at the eight corners of a cubic box (Figure S3).

The bonding pattern of σ plus π double delocalization renders three-dimensional aromaticity to the concerned chiral borospherene cations, as indicated by the negative nucleus-independent chemical shift (NICS)[42] values of −41 ppm and −40 ppm calculated for C_1 B_{41}^{+} (**1**) and C_2 B_{42}^{2+} (**2**) at the cage centers, respectively. These values are well comparable with the corresponding values of −43 ppm calculated for D_{2d} B_{40}, −42 ppm for D_{2d} B_{40}^{-}, and −38 ppm for C_3 B_{39}^{-} at the same theoretical level.[27,28]

Molecular dynamics (MD) simulations were performed for C_1 B_{41}^{+} (**1**) and C_2 B_{42}^{2+} (**2**) at 200, 300, and 500 K for 30 ps using the software suite CP2K.[43] As shown in Figure S4, both the C_1 B_{41}^{+} (**1**) and C_2 B_{42}^{2+} (**2**) species are dynamically stable at 200 K, with the small average root-mean-square-deviations of RMSD = 0.06 and 0.06 Å and maximum bond length deviations of MAXD = 0.26 and 0.23 Å, respectively. C_2 B_{42}^{2+}

© 2015 Wiley-VCH Verlag GmbH & Co. KGaA, Weinheim

(**2**) remains dynamically stable at both 300 and 500 K, similar to the observed D_{2d} B_{40}.[27] However, at 300 K and especially at 500 K, C_1 B_{41}^+ (**1**) exhibits obvious "stepped changes" in both RMSD and MAXD values (Figure S4a). Detailed analyses indicate that the monocation fluctuates almost barrierlessly between slightly different low-lying structures through concerted mechanisms during the simulation, similar to the dynamic behavior of the reported C_3/C_2 B_{39}^-,[28] further showing the size- and symmetry-dependence of the dynamics of boron clusters. Typical "snapshot" low-lying structures during the simulation all turn out to produce the same C_1 B_{41}^+ (**1**) global minimum when fully optimized. Both the low-symmetry C_1 B_{41}^+ and C_3/C_2 B_{39}^- are distorted from the perfect D_{2d} B_{40} due to the one-atom difference in cluster size, which gives rise to their structural fluctuations above room temperature. This observation further indicates the "glassy" nature of the low-symmetry borospherenes with odd number of boron atoms. Such cubic-box boron clusters (Figure S3) behave like a molecular "magic cube" (Rubik's cube) with numerous "barrierless" permutations.

Combination of the infrared photodissociation (IR-PD) spectroscopy and first-principles calculations has proven to be an effective approach in the characterizations of cluster cations.[44,45] We calculate here the vibrational frequencies and simulate the infrared (IR) spectra of C_1 B_{41}^+ (**1**) and C_2 B_{42}^{2+} (**2**) in Figure 4a, compared with the corresponding spectrum of the π-isovalent D_{2d} B_{40} at PBE0, which should facilitate their future IR-PD measurements. The detailed IR spectrum

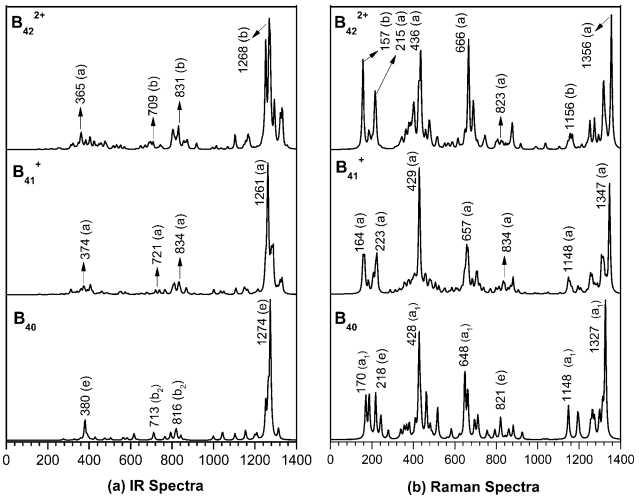

Figure 4. a) Simulated infrared and b) Raman spectra of C_1 B_{41}^+ (**1**) and C_2 B_{42}^{2+} (**2**) compared with those of the π-isovalent D_{2d} B_{40}, with typical vibrational frequencies indicated in cm^{-1}.

of D_{2d} B_{40} was discussed in previous reports.[29,30] As shown in Figure 4a, the simulated IR spectra of these borospherenes with different sizes, symmetries, and charge states exhibit obvious similarities in spectral features, with the four major IR peaks at 1274 cm^{-1} (e mode), 816 cm^{-1} (b_2 mode), 713 cm^{-1} (b_2 mode), and 380 cm^{-1} (e mode) in D_{2d} B_{40} well inherited in both C_1 B_{41}^+ (**1**) and C_2 B_{42}^{2+} (**2**). All the other IR active modes appear to be very weak.

The simulated Raman spectra of these borospherenes are presented in Figure 4b. Similar to IR spectra, their Raman spectra also appear to be insensitive to cage sizes, symmetries, and charge states. The seven major Raman peaks at 1327 cm^{-1} (a_1), 1148 cm^{-1} (a_1), 821 cm^{-1} (e), 648 cm^{-1} (a_1), 428 cm^{-1} (a_1), 218 cm^{-1} (e), and 170 cm^{-1} (a_1) in D_{2d} B_{40} are well maintained in both C_1 B_{41}^+(**1**) and C_2 B_{42}^{2+} (**2**). Among these Raman active modes, the two a_1 vibrations at 170 cm^{-1} and 428 cm^{-1} belong to typical "radial breathing modes" (RBMs) of the D_{2d} B_{40} cage. RBMs are used to identify the hollow structures in nanotubes. In the experimentally reported Raman spectrum of the single-walled boron nanotubes (which have the diameters of 36 ± 1 Å), an intense peak at 210 cm^{-1} was observed, which is typical for tubular structures and corresponds to the characteristic RBM mode.[46]

In summary, we have presented two new chiral members to the borospherene family using global minimum searches and first-principles calculations. The cage-like C_1 B_{41}^+ (**1**) and C_2 B_{42}^{2+} (**2**) are the global minima of the systems and probably viable for future experimental observations. The previously observed B_{39}^- and B_{40} and the currently predicted B_{41}^+ and B_{42}^{2+} (with the difference of a B^+ cation and a 3c–2e σ bond between two neighboring borospherenes) form a π-isovalent B_n^q series with twelve delocalized multicenter π bonds over a σ skeleton made of $n+8$ delocalized three-center σ bonds. The majority of these borospherenes are chiral species and they are all three-dimensional aromatic with the universal bonding pattern of σ plus π double delocalization. Chirality plays an important role in chemistry, materials science, and biology. The simulated infrared and Raman spectra of the two chiral borospherene cations invite experimental confirmations, which expand the borospherene family and may eventually lead to borospherene-based nanomaterials.

Methods Section

GM structural searches for B_{41}^+ and B_{42}^{2+} were performed using the minima hopping algorithm[9,32] at the DFT level, aided with manual structural constructions based on known boron clusters,[10–23,27,28] including typical planar, double- and triple-ring tubular, and cage-like initial structures. The MH calculations were carried out using the BigDFT electronic structure code,[47] which is based on a systematic wavelet basis in combination with pseudopotentials and the standard local-density approximation (LDA)[48] and Perdew–Burke–Ernzerhof (PBE)[49] exchange-correlation functionals. About 4890 and 4550 stationary points on the potential surfaces were probed for B_{41}^+ and B_{42}^{2+} in the MH searches, respectively. Low-lying structures were then fully optimized and their relative energies evaluated at both the hybrid density functional theory (DFT) levels PBE0[33] and CAM-B3LYP[34] with the 6-311+G* basis set[35] implemented in Gaussian 09 suite.[36] The relative stability of the two lowest-lying isomers are further calculated with the more accurate coupled cluster method with triple excitations (CCSD(T))[37–39] implemented in MOLPRO[40] using the 6-31G(d) basis set at the PBE0 geometries. Chemical bonding analyses were performed using the adaptive natural density partitioning (AdNDP) method[41] and visualized using the Molekel program.[50] Molecular dynamics (MD) simulations were done for C_1 B_{41}^+ (**1**) and C_2 B_{42}^{2+} (**2**) at 200, 300, and 500 K for 30 ps using the software suite CP2K.[43] The nucleus-independent chemical shifts (NICS)[42] at the cage centers were calculated to assess the three-dimensional aromaticity of these borospherene cations.

 © 2015 Wiley-VCH Verlag GmbH & Co. KGaA, Weinheim

Keywords: borospherene · first-principles theory · chirality · geometrical and electronic structures · delocalization

How to cite: *Angew. Chem. Int. Ed.* **2015**, *54*, 8160 – 8164
Angew. Chem. **2015**, *127*, 8278 – 8282

[1] H. W. Kroto, J. R. Heath, S. C. O'Brien, R. F. Curl, R. E. Smalley, *Nature* **1985**, *318*, 162 – 163.
[2] M. Monthioux, V. L. Kuznetsov, *Carbon* **2006**, *44*, 1621 – 1623.
[3] K. S. Novoselov, A. K. Geim, S. V. Morozov, D. Jiang, Y. Zhang, S. V. Dubonos, I. V. Grigorieva, A. A. Firsov, *Science* **2004**, *306*, 666 – 669.
[4] S. Bulusu, X. Li, L. S. Wang, X. C. Zeng, *Proc. Natl. Acad. Sci. USA* **2006**, *103*, 8326 – 8330.
[5] L. F. Cui, X. Huang, L. M. Wang, D. Y. Zubarev, A. I. Boldyrev, J. Li, L. S. Wang, *J. Am. Chem. Soc.* **2006**, *128*, 8390 – 8391.
[6] L. F. Cui, X. Huang, L. M. Wang, J. Li, L. S. Wang, *J. Phys. Chem. A* **2006**, *110*, 10169 – 10172.
[7] N. G. Szwacki, A. Sadrzadeh, B. I. Yakobson, *Phys. Rev. Lett.* **2007**, *98*, 166804.
[8] F. Y. Li, P. Jin, D. E. Jiang, L. Wang, S. B. Zhang, J. J. Zhao, Z. F. Chen, *J. Chem. Phys.* **2012**, *136*, 074302.
[9] S. Goedecker, W. Hellmann, T. Lenosky, *Phys. Rev. Lett.* **2005**, *95*, 055501.
[10] H. J. Zhai, A. N. Alexandrova, K. A. Birch, A. I. Boldyrev, L. S. Wang, *Angew. Chem. Int. Ed.* **2003**, *42*, 6004 – 6008; *Angew. Chem.* **2003**, *115*, 6186 – 6190.
[11] H. J. Zhai, B. Kiran, J. Li, L. S. Wang, *Nat. Mater.* **2003**, *2*, 827 – 833.
[12] B. Kiran, S. Bulusu, H. J. Zhai, S. Yoo, X. C. Zeng, L. S. Wang, *Proc. Natl. Acad. Sci. USA* **2005**, *102*, 961 – 964.
[13] A. P. Sergeeva, Z. A. Piazza, C. Romanescu, W. L. Li, A. I. Boldyrev, L. S. Wang, *J. Am. Chem. Soc.* **2012**, *134*, 18065 – 18073.
[14] W. Huang, A. P. Sergeeva, H. J. Zhai, B. B. Averkiev, L. S. Wang, A. I. Boldyrev, *Nat. Chem.* **2010**, *2*, 202 – 206.
[15] I. A. Popov, Z. A. Piazza, W. L. Li, L. S. Wang, A. I. Boldyrev, *J. Chem. Phys.* **2013**, *139*, 144307.
[16] E. Oger, N. R. M. Crawford, R. Kelting, P. Weis, M. M. Kappes, R. Ahlrichs, *Angew. Chem. Int. Ed.* **2007**, *46*, 8503 – 8506; *Angew. Chem.* **2007**, *119*, 8656 – 8659.
[17] W. L. Li, Y. F. Zhao, H. S. Hu, J. Li, L. S. Wang, *Angew. Chem. Int. Ed.* **2014**, *53*, 5540 – 5545; *Angew. Chem.* **2014**, *126*, 5646 – 5651.
[18] Z. A. Piazza, H. S. Hu, W. L. Li, Y. F. Zhao, J. Li, L. S. Wang, *Nat. Commun.* **2014**, *5*, 3113.
[19] A. P. Sergeeva, I. A. Popov, Z. A. Piazza, W. L. Li, C. Romanescu, L. S. Wang, A. I. Boldyrev, *Acc. Chem. Res.* **2014**, *47*, 1349 – 1358.
[20] W. L. Li, Q. Chen, W. J. Tian, H. Bai, Y. F. Zhao, H. S. Hu, J. Li, H. J. Zhai, S. D. Li, L. S. Wang, *J. Am. Chem. Soc.* **2014**, *136*, 12257 – 12260.
[21] Q. Chen, G. F. Wei, W. J. Tian, H. Bai, Z. P. Liu, H. J. Zhai, S. D. Li, *Phys. Chem. Chem. Phys.* **2014**, *16*, 18282 – 18287.
[22] W. L. Li, C. Romanescu, T. Jian, L. S. Wang, *J. Am. Chem. Soc.* **2012**, *134*, 13228 – 13231.
[23] D. Z. Li, Q. Chen, Y. B. Wu, H. G. Lu, S. D. Li, *Phys. Chem. Chem. Phys.* **2012**, *14*, 14769 – 14774.
[24] I. Boustani, *ChemPhysChem* **2005**, *6*, 2001 – 2008.
[25] H. Tang, S. Ismail-Beigi, *Phys. Rev. Lett.* **2007**, *99*, 115501.
[26] X. B. Yang, Y. Ding, J. Ni, *Phys. Rev. B* **2008**, *77*, 041402.
[27] H. J. Zhai, Y. F. Zhao, W. L. Li, Q. Chen, H. Bai, H. S. Hu, Z. A. Piazza, W. J. Tian, H. G. Lu, Y. B. Wu, Y. W. Mu, G. F. Wei, Z. P. Liu, J. Li, S. D. Li, L. S. Wang, *Nat. Chem.* **2014**, *6*, 727 – 731.
[28] Q. Chen, W. L. Li, Y. F. Zhao, S. Y. Zhang, H. S. Hu, H. Bai, H. R. Li, W. J. Tian, H. G. Lu, H. J. Zhai, S. D. Li, J. Li, L. S Wang, *ACS Nano* **2015**, *9*, 754 – 760.
[29] H. Bai, Q. Chen, H. J. Zhai, S. D. Li, *Angew. Chem. Int. Ed.* **2015**, *54*, 941 – 945; *Angew. Chem.* **2015**, *127*, 955 – 959.
[30] R. X. He, X. C. Zeng, *Chem. Commun.* **2015**, *51*, 3185 – 3188.
[31] P. Jin, Q. H. Hou, C. C. Tang, Z. F. Chen, *Theor. Chem. Acc.* **2015**, *134*, 13 – 22.
[32] S. Goedecker, *J. Chem. Phys.* **2004**, *120*, 9911 – 9917.
[33] C. Adamo, V. Barone, *J. Chem. Phys.* **1999**, *110*, 6158 – 6170.
[34] T. Yanai, D. Tew, N. Handy, *Chem. Phys. Lett.* **2004**, *393*, 51 – 57.
[35] R. Krishnan, J. S. Binkley, R. Seeger, J. A. Pople, *J. Chem. Phys.* **1980**, *72*, 650 – 654.
[36] Gaussian 09, Revision A.2, M. J. Frisch, et al., Gaussian Inc., Wallingford, CT, **2009**.
[37] J. Čížek, *Adv. Chem. Phys.* **1969**, *14*, 35 – 89.
[38] G. D. Purvis, R. J. Bartlett, *J. Chem. Phys.* **1982**, *76*, 1910 – 1918.
[39] K. Raghavachari, G. W. Trucks, J. A. Pople, M. Head-Gordon, *Chem. Phys. Lett.* **1989**, *157*, 479 – 483.
[40] H. J. Werner, et al. MOLPRO, version **2012**.1.
[41] D. Yu. Zubarev, A. I. Boldyrev, *Phys. Chem. Chem. Phys.* **2008**, *10*, 5207 – 5217.
[42] P. v. R. Schleyer, C. Maerker, *J. Am. Chem. Soc.* **1996**, *118*, 6317 – 6318.
[43] J. VandeVondele, M. Krack, F. Mohamed, M. Parrinello, T. Chassaing, J. Hutter, *Comput. Phys. Commun.* **2005**, *167*, 103 – 108.
[44] G. J. Wang, J. M. Cui, C. X. Chi, X. J. Zhou, Z. H. Li, X. P. Xing, M. F. Zhou, *Chem. Sci.* **2012**, *3*, 3272 – 3279.
[45] G. J. Wang, M. F. Zhou, J. T. Goettel, G. J. Schrobilgen, J. Su, J. Li, T. Schloder, S. Riedel, *Nature* **2014**, *514*, 475 – 477.
[46] D. Ciuparu, R. F. Klie, Y. M. Zhu, L. Pfefferle, *J. Phys. Chem. B* **2004**, *108*, 3967 – 3969.
[47] L. Genovese, A. Neelov, S. Goedecker, T. Deutsch, S. A. Ghasemi, A. Willand, D. Caliste, O. Zilberberg, M. Rayson, A. Bergman, R. Schneider, *J. Chem. Phys.* **2008**, *129*, 014109.
[48] S. Goedecker, M. Teter, J. Hutter, *Phys. Rev. B* **1996**, *54*, 1703 – 1710.
[49] J. P. Perdew, K. Burke, M. Ernzerhof, *Phys. Rev. Lett.* **1996**, *77*, 3865 – 3868.
[50] U. Varetto, Molekel 5.4.0.8, Swiss National Supercomputing Centre, Manno, Switzerland, **2009**.

Received: February 17, 2015
Published online: May 26, 2015

© 2015 Wiley-VCH Verlag GmbH & Co. KGaA, Weinheim